BIG DATA MINING AND ANALYTICS
ISSN 2096-0654 05/10 pp44–54
Volume 6, Number 1, March 2023
DOI: 10.26599/BDMA.2022.9020027

Satellite Image Classification Using a Hybrid Manta Ray Foraging Optimization Neural Network

Amit Kumar Rai*, Nirupama Mandal, Krishna Kant Singh, and Ivan Izonin

Abstract: A semi supervised image classification method for satellite images is proposed in this paper. The satellite images contain enormous data that can be used in various applications. The analysis of the data is a tedious task due to the amount of data and the heterogeneity of the data. Thus, in this paper, a Radial Basis Function Neural Network (RBFNN) trained using Manta Ray Foraging Optimization algorithm (MRFO) is proposed. RBFNN is a three-layer network comprising of input, output, and hidden layers that can process large amounts. The trained network can discover hidden data patterns in unseen data. The learning algorithm and seed selection play a vital role in the performance of the network. The seed selection is done using the spectral indices to further improve the performance of the network. The manta ray foraging optimization algorithm is inspired by the intelligent behaviour of manta rays. It emulates three unique foraging behaviours namelys chain, cyclone, and somersault foraging. The satellite images contain enormous amount of data and thus require exploration in large search space. The spiral movement of the MRFO algorithm enables it to explore large search spaces effectively. The proposed method is applied on pre and post flooding Landsat 8 Operational Land Imager (OLI) images of New Brunswick area. The method was applied to identify and classify the land cover changes in the area induced by flooding. The images are classified using the proposed method and a change map is developed using post classification comparison. The change map shows that a large amount of agricultural area was washed away due to flooding. The measurement of the affected area in square kilometres is also performed for mitigation activities. The results show that post flooding the area covered by water is increased whereas the vegetated area is decreased. The performance of the proposed method is done with existing state-of-the-art methods.

Key words: Radial Basis Function Neural Network (RBFNN); Manta Ray Foraging Optimization algorithm (MRFO); Landsat 8; classification; change detection; disaster mitigation; planning

1 Introduction

Satellite image classification is being used in multiple areas like climate change detection, urban planning, monitoring, and disaster mitigation, and so on. The satellite image classification is a complex problem due to the nature of the data. The satellite images have

• Amit Kumar Rai is with the Department of Electronics Engineering, Indian Institute of Technology, Dhanbad (ISM, Dhanbad), Dhanbad 826004, India, and also with the Department of Electronics and Communication Engineering, Asansol Engineering College, Asansol 713305, India. E-mail: amitrai2212@gmail.com.
• Nirupama Mandal is with the Department of Electronics Engineering, Indian Institute of Technology, Dhanbad (ISM, Dhanbad), Dhanbad 826004, India.
• Krishna Kant Singh is with the Department of CSE, ASET, Amity University, Noida 201301, India. E-mail: krishnaiitr2011@gmail.com.
• Ivan Izonin is with the Department of Artificial Intelligence, Lviv Polytechnic National University, Lviv 79000, Ukraine. E-mail: ivan.v.izonin@lpnu.ua.
* To whom correspondence should be addressed.
Manuscript received: 2022-05-15; revised: 2022-07-11; accepted: 2022-07-18

enormous amount of underlying data in form of pixels and different spectral bands. Each pixel represents a point on the land and contains the information about that point. Each pixel may represent an area of few meters to multiple kilometres based on the resolution of the imagery. The satellite image classification algorithm should therefore be informative, exhaustive, and separable[1]. Satellite image classification is used for obtaining the land cover mapping of the area captured in the imagery. Land cover pattern provides important information for identification and analysis of many natural phenomenon on Earth. In modern era, satellite image plays a vital role for identification, assessment, and mitigation planning of natural hazards. Conventionally, ground inspection and field survey were used for these activities. In the event of a natural hazard, it is quite difficult to visit the place of disaster physically and cover broad area in short span of time by such conventional methods. Thus, satellite images are being effectively used for detecting land cover change, urban planning, and disaster mitigation. With the use of satellite images, the disaster planners can monitor large areas without the need of visiting the actual site. Floods are the most frequent destructive disaster which causes large scale damage in agricultural land and urban areas every year. Flood is the primary reason of the damage of ecological resources, the lack of food, the starvation of numerous million people, and the massive economic losses. The vegetated areas and farms that are in the vicinity of water bodies are significantly affected by flooding. The flooding causes enormous loss of agricultural cultivated lands. Thus, one of the primary concerns of different countries is to detect flood affected areas so that the effects of floods can be mitigated swiftly. Multi-temporal remote sensing images are utilized for identification of alterations in urban areas, forestation, and flooding[2–4]. Pre and post Landsat 7 ETM satellite images of flood affected area were used to classify these bi-temporal images to identify flooded area[5]. The difference of backscattering coefficients from the bi-temporal TerraSAR-X intensity images of the 2011 Japan tsunami were used for identifying affected flooded areas and collapsed and damaged buildings[6]. Normalized water index, normalized vegetation index, and normalized difference surface water index (spectral indices of Landsat images of disaster) are used to prepare maps of flood extent[7]. Independent Component Analysis (ICA) was used on bi-temporal flood images to detect changes. Water pixels were extracted using image classification and the cloud and irrigated agricultural areas were masked to obtain refine result[8].

An integrated method was proposed that used Normalized Difference Flood Index-3 (NDFI3) on Landsat 8 Operational Land Imager (OLI) TIRS to estimate the impact of inundation in Malaysia[9]. Artificial Neural Network (ANN) based methods have been applied for satellite image classification problem. These neural networks are broadly categorized into supervised classification. These neural networks are hybridized with fuzzy and meta-heuristic optimization for more accurate image classification[10–13]. An effective neuro-fuzzy GIFKCN classifier was used to detect the 2011 Tohoku tsunami inundated area. GIFKCN is the hybridization of Generalized Improved Fuzzy Partitions FCM (GIFP-FCM) and Kohonen clustering network, having the advantages of both a fuzzy and neural network[13]. A recent unsupervised change detection method detects the changes between bi-temporal satellite images using Radial Basis Function (RBF)/GIFP-FCM and wavelet fusion[14].

In this paper, a novel and efficient technique that uses Radial Basis Function Neural Network (RBFNN) and Manta Ray Foraging Optimization Algorithm (MRFO) is proposed. Spectral indices are being used for seed selection of the network and MRFO is used to train the RBFNN. The proposed method improves the seed selection and exploration property of the network. The training using MRFO improves the network efficiency. This method is applied to detect inland flooding in the maritime province, New Brunswick, on the east coast of Canada. In May 2018, the combination of heavy rainfall and melting snow caused the disastrous flooding along the St. John River, New Brunswick. Pre and post Landsat8 OLI satellite images are being used for classification using hybrid MRFO-RBFNN. The classified images are used to detect the changes in water class and make the flood map. The changes that have occurred due to flooding are highlighted in the result. The change detection map is created using post classification comparison. The change map represents the changes in the land cover due to flooding.

This paper is organized in eight sections. Section 1 gives an introduction about the research problem and literature review. In Section 2, the background about the work is given including radial basis function neural network and manta ray foraging optimization algorithm. Section 3 describes the site description and dataset used. Section 4 explains the training procedure using MRFO

algorithm. This is followed by the methodology in Section 5. Section 6 discusses the accuracy assessment of the proposed method. Section 7 comprises of result analysis. Section 8 gives the conclusion of the proposed work.

2 Background

2.1 Radial basis function neural network

A Radial Basis Function (RBF) network is a classification and functional approximation feed forward network developed by M. J. D. Powell. This neural network uses the most common nonlinearities such as sigmoid and Gaussian kernel function[15]. The architecture of RBFNN consists of three layers which are shown in Fig. 1. The input layer is the first layer of the network which communicates and connects the external inputs to the neural network. After the inputs are being processed, the output is mapped on the output layers. The most significant part of the network is the hidden layer which is placed in between input and output layers. The hidden layer implements the Radial Basis Function (RBF). The RBFs generate activations; the strength of the activations produced is inversely proportional to the distance of the node from the centre.

The RBFs are represented by the nodes of the hidden layer with the centre on a vector in the feature space. A node at the hidden layer gets input as the n dimensional input vector χ. The radial centres are denoted by $\zeta_1, \zeta_2, \ldots, \zeta_\lambda$.

Equation (1) provides the output of the j-th hidden layer.

$$\psi_j = \psi\left(\|\chi - \zeta_j\|\right) = \exp\left(-\frac{\|\chi - \zeta_j\|^2}{2\sigma_j^2}\right) \quad (1)$$

where χ is the input vector and can be defined mathematically as $\chi = \{x_1, x_2, \ldots, x_N\}$. $\psi(\cdot)$ represents the RBF. $\|\ \|$ is used to specify that the

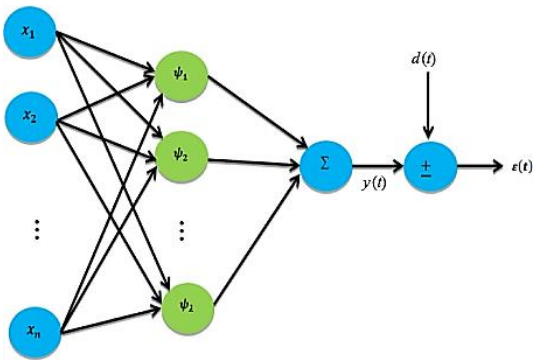

Fig. 1 Architecture of RBFNN.

subtraction is not simple. It is the Euclidean distance and amid the input and the j-th cluster centre. σ_j represents the standard deviation of the j-th Gaussian function. The mathematical representation of the standard deviation is given in Eq. (2).

$$\sigma = \nabla_{\max}/\sqrt{\lambda} \quad (2)$$

where $\nabla_{\max}$ represents the highest distance amid the centres. The RBFNN output y is given as

$$y = \sum_{j=1}^{\lambda} w_j \cdot \psi\left(\|\chi - \zeta_j\|\right) \quad (3)$$

where λ represents the count of cluster centres and w_j is the weight of the j-th hidden unit. The weights of RBF network are updated by network training. The fitness value of the generated MRFO agents is measured using the least square error. It is used for computing the variation in the actual and predicted values obtained by the RBFNN for the training samples. The least square error can be calculated by

$$\varepsilon(t) = \frac{1}{2}(d(t) - y(t))^2 \quad (4)$$

where $d(t)$ represents the desired output whereas $y(t)$ is the obtained output form the network.

2.2 Manta ray foraging optimization algorithm

Manta ray foraging optimization algorithm is a novel bio inspired optimization technique. The algorithm is based on the activities of manta rays that resemble the activities of foraging like chaining, cyclone, and somersault[16]. The algorithm is used to solve highly complex optimization problems. The different chaining strategies are used to update the positions of the manta rays to find the best foodstuff. Thereafter, the swarm follows a cyclonic path and swims in spiral manner. The mathematical modelling of this behaviour is discussed in this section.

Chain foraging: In search of food, the manta rays swim towards plankton. The plankton with the highest concentration is assumed to be the best food and thus all manta rays swim towards it. While reaching towards the best food, the manta rays move one behind the other in a head to tail manner. Thus, each manta ray not only moves towards the best food but also follows its previous manta ray. In chain foraging, the manta rays swim in a spiral way towards the food. Figure 2 shows the foraging behaviour. This is analogous to an optimization problem where the position is updated using the best solution and its previous solution. This modelling is represented in Eq. (5).

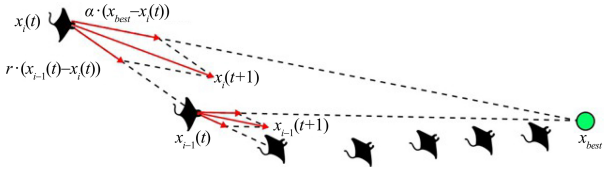

Fig. 2 MRFO: Chain foraging.

$$x_i^d\ (t+1) = \begin{cases} x_i^d\ (t) + r\cdot\left(x_{best}^d\ (t) - x_i^d\ (t)\right) + \\ \quad \alpha\cdot\left(x_{best}^d\ (t) - x_i^d\ (t)\right), \ \ i=1; \\ x_i^d\ (t) + r\cdot\left(x_{i-1}^d\ (t) - x_i^d\ (t)\right) + \\ \quad \alpha\cdot\left(x_{best}^d\ (t) - x_i^d\ (t)\right), \ \ i=2,3,\ldots,N \end{cases} \tag{5}$$

$$\alpha = 2\cdot r\cdot\sqrt{|\log(r)|} \tag{6}$$

where $x_i^d(t)$ is the position of the i-th individual at time t in the d-th dimension, r is the random number in [0,1], α is the weight coefficient, and x_{best}^d is the best solution.

Cyclone foraging: Along with the spiral movement like that in chain foraging, another movement is also followed by manta rays. The second kind of movemnt is cyclone foraging. In this, the manta rays swim to follow the particles ahead them. This kind of foraging behavior is depicted in Fig. 3. This movement is mathematically represented in Eq. (7).

$$\begin{cases} X_i\ (t+1) = X_{best} + r\cdot(X_{i-1}\ (t) - X_i\ (t)) + \\ \qquad e^{bw}\cdot\cos(2\pi w)\cdot(X_{best} - X_i\ (t)), \\ Y_i\ (t+1) = Y_{best} + r\cdot(Y_{i-1}\ (t) - Y_i\ (t)) + \\ \qquad e^{bw}\cdot\cos(2\pi w)\cdot(Y_{best} - Y_i\ (t)) \end{cases} \tag{7}$$

where w is the random number in [0,1].

Equation (7) can be generalized for n-D space as follows:

$$x_i^d\ (t+1) = \begin{cases} x_{best}^d + r\cdot\left(x_{best}^d\ (t) - x_i^d\ (t)\right) + \\ \beta\cdot\left(x_{best}^d\ (t) - x_i^d\ (t)\right), \ \ i=1; \\ x_{best}^d + r\cdot\left(x_{i-1}^d\ (t) - x_i^d\ (t)\right) + \\ \beta\cdot\left(x_{best}^d\ (t) - x_i^d\ (t)\right), \ \ i=2,3,\ldots,N \end{cases} \tag{8}$$

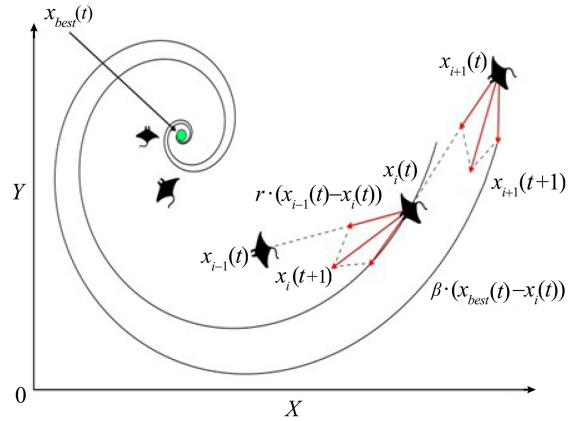

Fig. 3 MRFO cyclone foraging.

$$\beta = 2e^{r_1\frac{T-I+1}{r}}\cdot\sin(2\pi r_1) \tag{9}$$

where β is the weight coefficient, T is the number of epochs, and r is the random number in [0, 1].

With cyclone foraging, the ability to explore a large search space is improved as the manta rays explore the best food. This behaviour is significant in solving complex optimization problems where the search space is large. The large space becomes searchable due to the cyclone foraging behaviour. The mathematical representation of this searching behaviour is as follows:

$$x_{rand}^d = Lb^d + r\cdot(Ub^d - Lb^d),$$

$$x_i^d\ (t+1) = \begin{cases} x_{rand}^d + r\cdot\left(x_{rand}^d - x_i^d\ (t)\right) + \beta\cdot \\ \quad \left(x_{rand}^d - x_i^d\ (t)\right), \ \ i=1; \\ x_{rand}^d + r\cdot\left(x_{i-1}^d\ (t) - x_i^d\ (t)\right) + \beta\cdot \\ \quad \left(x_{rand}^d\ (t) - x_i^d\ (t)\right), \ \ i=2,3,\ldots,N \end{cases} \tag{10}$$

where x_{rand}^d is random position, and Lb^d and Ub^d are lower and upper bounds, respectively.

Somersault foraging: The manta rays also show a somersault foraging behaviour. The manta rays swim towards the food and backwards to a new position. The manta rays somersault while swimming from food towards another position. Figure 4 shows this behaviour. This behaviour is modelled using Eq. (11).

$$x_i^d\ (t+1) = x_i^d\ (t) + S\cdot(r_2\cdot x_{best}^d - r_3\cdot x_i^d\ (t)), \ \ i=1,2,\ldots,N \tag{11}$$

where S is somersault factor, and r_2 and r_3 are random numbers in [0, 1].

3 Site Description and Satellite Data Used

Landsat 8 Operational Land Imager (OLI) images of New Brunswick area are used for applying the proposed classifier[17]. The OLI sensor acquires images in the visible wavelength with 30 m multispectral resolution and 15 m resolution for panchromatic band. The band information of the sensor is given in Table 1.

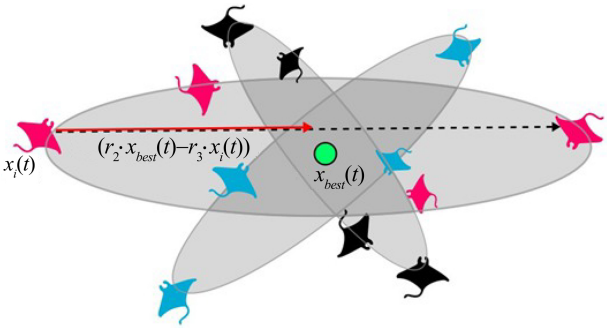

Fig. 4 MRFO somersault foraging.

Table 1 Landsat 8 OLI spectral bands.

Band	Wavelength (m)	Resolution (m)
Band 1—Coastal aerosol	0.43–0.45	30
Band 2—Blue	0.45–0.51	30
Band 3—Green	0.53–0.59	30
Band 4—Red	0.64–0.67	30
Band 5—Near infrared (NIR)	0.85–0.88	30
Band 6—SWIR 1	1.57–1.65	30
Band 7—SWIR2	2.11–2.29	30

The medium resolution images of Landsat 8 OLI are well suited by land classification to cover large areas in a single image. The area selected is New Brunswick located on the east coast of Canada and was hard hit by flooding in May, 2018. The continuous melting of snow combined with heavy rainfall resulted in flooding along the St. John river. The images acquired before and after the flooding are used in this paper. The pre flooding image acquired on 22nd Oct 2017 and post flooding image acquired on 18th May 2018 by Landsat 8 OLI are used (Fig. 5).

4 Training Using MRFO

In this paper, the training of the RBFNN is proposed using manta ray foraging optimization algorithm. The foraging behaviour of MRFO improves the efficiency of the network. Satellite images contain a large amount of data and consequently for finding optimal centres a large search space needs to be explored. The spiral movement and the three different foraging behaviours of manta rays enable the network to explore the search space. Thus, the proposed method works efficiently in satellite image classification. The RBFNN is trained using MRFO (MRFO-RBFNN) for finding optimal cluster centres. The network has a single hidden layer. The search agent is represented as a one dimensional vector to represent the RBFNN. Using MRFO the weights of the neurons are updated using chain, cyclone, and somersault foraging. The proposed training algorithm is as Algorithm 1.

5 Methodology

In the proposed methodology, satellite image classification is done using multispectral satellite images. The method takes a multispectral image as input and produces the classified image using MRFO-RBFNN. Pre and post flooding images are classified into the required classes. The classified images are compared using post classification comparison. Figure 6 shows the flowchart of the proposed method.

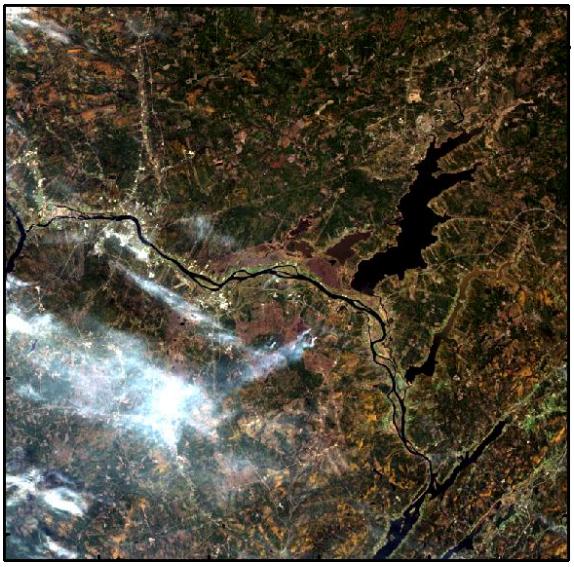

(a) Pre flooding

(b) Post flooding

Fig. 5 Pre and post flooding Landsat 8 OLI images of the study area.

5.1 Image pre-processing

The multi-temporal image analysis based on quantities comparison requires that the images used for comparison should not have any effect of acquisition conditions. Image processing is done to fulfil this requirement. The digital numbers are transformed to reflectance values. This will overcome the difference in brightness of the images. The brightness differences are due to the varied illumination conditions and sun angle during image acquisition. The sensor calibrations also contribute to the variations in the brightness of the temporal images. Therefore, in this paper the pixel values are converted

Algorithm 1 Training with MRFO

Begin

Initialization: Initialize the population N_{pop}, $t_{\max}$, and somersault factor (sf) , randomly initialize manta rays with λ random cluster centres using

$x_i(t) = x_l + rand(x_u - x_l)$ for $i = 1, 2, \ldots, N_{pop}$ and $t = 1$

where $[x_u, x_l]$ is the range of the problem space.

Fitnes computation: Compute fitness of each manta ray and find best solution, x_{best}

Weight updation:

while $t < t_{\max}$

for $i = 1$ to N_{pop}

if $rand < 0.5$

Apply cyclone foraging

if $t/t_{\max} < rand$

$x_{rand} = x_l + rand \cdot (x_u - x_l)$

$x_i(t+1) =$

$$\begin{cases} x_{rand} + r \cdot (x_{rand} - x_i(t)) + \beta (x_{rand} - x_i(t)), i = 1; \\ x_{rand} + r \cdot (x_{i-1}(t) - x_i(t)) + \beta (x_{rand} - x_i(t)), \\ \quad i = 2, 3, \ldots, N_{pop} \end{cases}$$

Else

$x_i(t+1) =$

$$\begin{cases} x_{best} + r \cdot (x_{best} - x_i(t)) + \beta (x_{best} - x_i(t)), i = 1; \\ x_{best} + r \cdot (x_{i-1}(t) - x_i(t)) + \beta (x_{best} - x_i(t)), \\ \quad i = 2, 3, \ldots, N_{pop} \end{cases}$$

End If

Else

Apply Chain foraging

$x_i(t+1) =$

$$\begin{cases} x_i(t) + r \cdot (x_{best} - x_i(t)) + \alpha (x_{best} - x_i(t)), i = 1; \\ x_i(t) + r \cdot (x_{i-1}(t) - x_i(t)) + \alpha (x_{best} - x_i(t)), \\ \quad i = 2, 3, \ldots, N_{pop} \end{cases}$$

End if

Compute fitness value for each manta ray.

Update x_{best} if $x_i(t+1) > x_{best}$

Apply somersault foraging

for $i = 1$ to N_{pop}

$x_i(t+1) = x_i(t) + S \cdot (r_2 \cdot x_{best} - r_3 \cdot x_i(t))$

end for

Compute fitness value for each manta ray.

Update x_{best} if $x_i(t+1) > x_{best}$

End for

Termination:

End while

Output best solution

to the corresponding reflectance value, i.e., the top of atmosphere reflectance (ρ_{TOA}) is computed.

5.2 Feature extraction using spectral indices

Remote sensing researchers use a number of spectral indices to predict or identify a particular type of land cover. These indices are widely used for monitoring vegetation, water, soil, etc. The ratio of near infrared and visible bands is significant in obtaining vegetation features. On computing this ratio, the vegetated areas get higher values whereas other land cover types get low

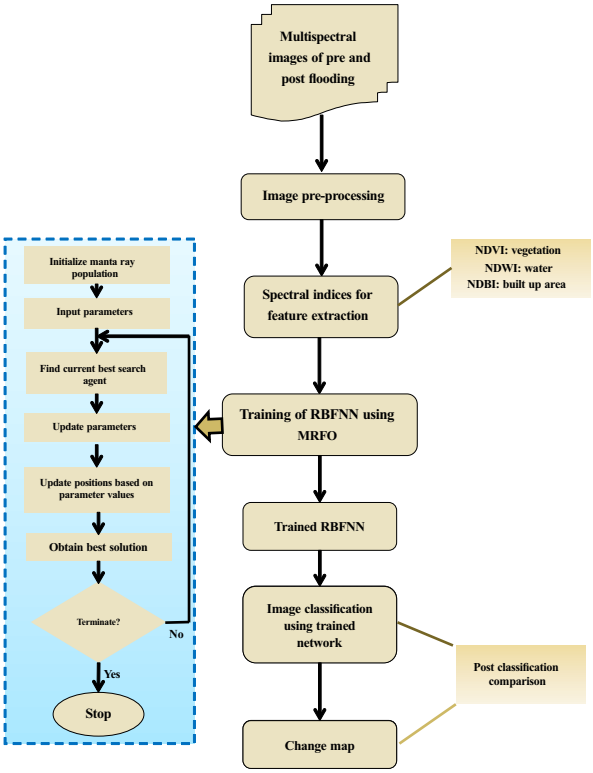

Fig. 6 Flow chart of the proposed method.

values. The different spectral indices are summarized in Table 2.

The feature extraction in this paper is done using the spectral indices. The spectral indices used here include Normalized Difference Vegetation Index (NDVI), Normalized Difference Water Index (NDWI), and Normalized Difference Built up Index (NDBI). NDVI is commonly used to highlight vegetation areas in an image[18–21].

NDVI uses the NIR and red band to find the vegetation index. The spectral signature of the vegetated area is that it absorbs the visible light, however, the NIR is reflected

Table 2 Spectral indices.

No.	Index	Mathematical equation
1	Normalized Difference Water Index (NDWI)	$I_{NDWI} = \frac{\psi_{green} - \psi_{nir}}{\psi_{green} + \psi_{nir}}$
2	Modified Normalized Difference Water Index (MNDWI)	$I_{MNDWI} = \frac{\psi_{green} - \psi_{mir}}{\psi_{green} + \psi_{mir}}$
3	Normalized Difference Vegetation Index (NDVI)	$I_{NDVI} = \frac{\psi_{nir} - \psi_{red}}{\psi_{nir} + \psi_{red}}$
4	Soil Adjusted Vegetation Index (SAVI)	$I_{SAVI} = \frac{(\psi_{nir} - \psi_{red}) \times (1+L)}{(\psi_{nir} + \psi_{red} + L)}$ where L is the soil correction factor.
5	Normalized Difference Building Index (NDBI)	$I_{NDBI} = \frac{\psi_{mir} - \psi_{nir}}{\psi_{mir} + \psi_{nir}}$

back. This property is used to compute the vegetation index. The index is computed using Eq. (12).

$$I_{NDVI} = \frac{\psi_{nir} - \psi_{red}}{\psi_{nir} + \psi_{red}} \tag{12}$$

The water bodies and snow areas are captured using the water index. This index utilizes the green and NIR bands. In NDWI, the water pixels have high positive values whereas other features have zero or negative values[18]. This can be computed using Eq. (13).

$$I_{NDWI} = \frac{\psi_{green} - \psi_{nir}}{\psi_{green} + \psi_{nir}} \tag{13}$$

The features of built up area is computed using the NDBI. It uses the MIR and NIR band of the imagery. The mathematical equation to compute NDBI is given in Eq. (14).

$$I_{NDBI} = \frac{\psi_{mir} - \psi_{nir}}{\psi_{mir} + \psi_{nir}} \tag{14}$$

where $\psi_{nir}, \psi_{red}, \psi_{mir}$, and ψ_{green} are the spectral bands corresponding to near infrared, red, mid infrared, and green light, respectively. The indices obtained are in gray scale, thus to get the intensity level that best describes the features, histogram techniques is used. A histogram is defined as plot of the intensity versus the pixel count data. The histograms of the spectral indices are computed and the central value of the histogram is used as the initial cluster centre for the respective classes. The indices computed for the pre and post flooding images along with their histograms are shown in Fig. 7.

5.3 MRFO-RBFNN for image classification

5.3.1 Initialization

In the first step, the network parameters are initialized. The number of hidden nodes is set to λ. Random initialization of node weights is done uniformly around

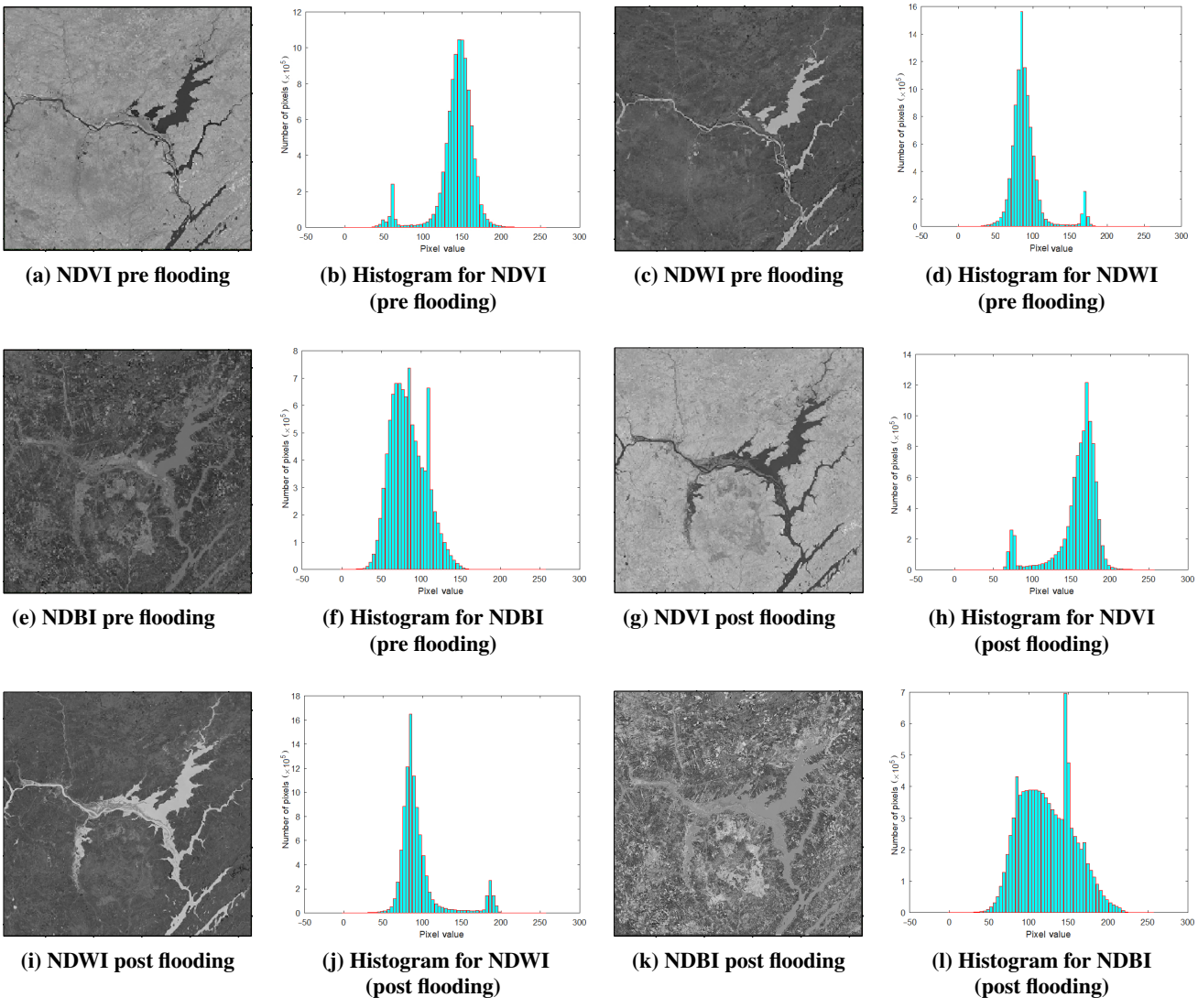

(a) NDVI pre flooding (b) Histogram for NDVI (pre flooding) (c) NDWI pre flooding (d) Histogram for NDWI (pre flooding)

(e) NDBI pre flooding (f) Histogram for NDBI (pre flooding) (g) NDVI post flooding (h) Histogram for NDVI (post flooding)

(i) NDWI post flooding (j) Histogram for NDWI (post flooding) (k) NDBI post flooding (l) Histogram for NDBI (post flooding)

Fig. 7 Spectral indices with their histograms.

0 and the empirical variance of 0.2.

5.3.2 Centre computation

The features extracted from the spectral indices are fed into the MRFO which in turn trains the network to output the updated centres.

5.3.3 Fitness evaluation

The fitness evaluation is the most important step for network termination and accurate classification. Improperly used termination will lead to inappropriate iterations which in turn lead to over fitting of the network. The ill effect of over fitting is divergence. Mean Square Error (*MSE*) is used to compute the fitness, it can be computed using Eq. (15).

$$MSE = \frac{1}{n}\sum(d\,(t) - y(t))^2 \qquad (15)$$

where n is the number of instances in the training dataset. The aim is to minimize the *MSE* by updating the cluster centers using the training dataset.

The trained MRFO-RBFNN is now applied on the bi-temporal images to classify them into the desired classes as shown in Fig. 8. The change map shown in Fig. 8c is developed from the classified images by applying post classification comparison.

5.4 Change detection

Post Classification Comparison (PCC) is done to obtain a set of four change classes. The change classes are used to produce a classified map. The class-by-class comparison of the classified images is performed. The changes in various classes are observed and stored. This technique can find changes easily and in an efficient manner. The change detection is done using PCC. The pixel wise comparison of the pre and post classified image is done. If the classes of both pre and post classified images are same, then there is no change else a change is registered.

If $C_1\,(i,j) = C_2\,(i,j)$ then no change,

If $C_1\,(i,j) \neq C_2\,(i,j)$ then change detected,

where $C_1\,(i,j)$ is the class of pixel at (i,j) in pre classified images, and $C_2\,(i,j)$ is the $i\,(i,j)$ in post classified images.

6 Accuracy Assessment and Detection of Flooded Area

The accuracy assessment is a tool that helps in understanding the correctness of the method proposed. The confusion matrix is used along with the other metrics

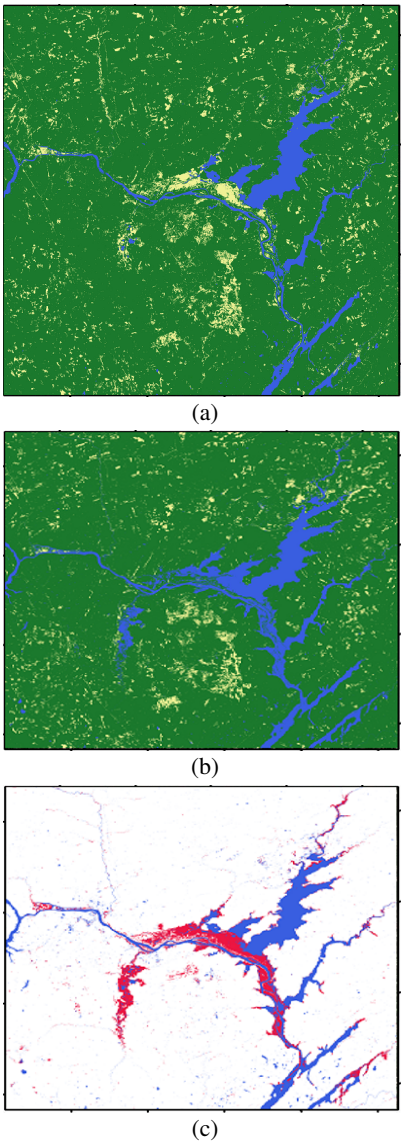

Fig. 8 Classified images. (a) Pre flooding; (b) Post flooding; (c) Change map.

like kappa coefficient and overall accuracy is used[22]. The correctness of the accuracy assessment depends on the selection of the sample points for computing the accuracy measures. In most of the previous works, the training data are used for sampling and calculation. But these data are not suitable for the assessment task as the training data are not purely random and also they are influenced by the programmer's biases. Therefore, stratified random technique for sample selection is used. The accuracy assessment methods available in ERDAS software are used for computing the accuracy. The stratified random technique randomly selects sample points from each class. Thereafter, a confusion matrix is made to give information about the correctly identified and wrongly identified points

in the results. The assessment results of the pre and post flooding images are summarized in Tables 3–6. Pre and post flooding images have an overall accuracy of 98.05% and 98.44%, respectively. The kappa values obtained approach 1 which implies the effectiveness of the proposed method. The values obtained are 0.96 and 0.97 for pre and post images, respectively. The other states of the art methods are used for comparison. The comparative results are summarized in Table 7.

7 Result Analysis

The image used is a subset image covering of size 3075 pixel × 3124 pixel. The spatial resolution of the image is 30 m thus each pixel covers an area of (30 × 30) m^2. The total area covered by the study image is therefore 8645.7 km^2. The image is classified into three classes, water, built up area including barren lands, and vegetation. From the classified image obtained using the proposed method, the area covered by each class is shown in Table 8. Figure 9 shows the overall accuracy of the proposed method with other state-of-the-art methods.

Thus, it can be seen that due to the flooding, the water area has increased from 5% to 8% post flooding that is approximately 243.73 km^2 of area, as shown in Fig. 10. The increase in water has led to the destruction of built up and vegetation area. The reduction in vegetation is seen to be of 2% that is an area of 153.74 km^2. The vegetated area is washed away by the flood leading to high losses of agricultural land. The built-up and barren land area have also reduced by 1% that is an area of 89.94 km^2 due to flooding.

Table 3 Confusion matrix for pre flooding image.

Reference data	Water	Vegetation	Urban	Total
Water	**39**	0	1	40
Vegetation	1	**172**	1	174
Urban	0	2	**40**	42
Total	40	174	42	**256**

Table 4 Accuracy results for pre flooding image.

Class name	Producer's accuracy (%)	User's accuracy (%)	Conditional kappa
Water	97.50	97.50	0.97
Vegetation	98.85	98.85	0.96
Urban	95.24	95.24	0.94

Note: Overall accuracy: 98.05%, overall kappa: 0.96.

Table 5 Confusion matrix for post flooding image.

Reference data	Water	Vegetation	Urban	Total
Water	**39**	0	1	40
Vegetation	1	**138**	0	139
Urban	0	2	**75**	77
Total	40	140	76	**256**

Table 6 Accuracy results for post flooding image.

Class name	Producer's accuracy (%)	User's accuracy (%)	Conditional kappa
Water	97.50	97.50	0.97
Vegetation	98.57	99.28	0.98
Urban	98.68	97.40	0.96

Note: Overall accuracy: 98.44%, overall kappa: 0.97.

Table 7 Accuracy and kappa.

Image	Method	Overall accuracy (%)	Kappa
Pre flooding	FCM	95.70	0.91
	GIFP-FCM	96.48	0.93
	FKLICM	96.88	0.94
	MRFO-RBFNN	98.05	0.96
Post flooding	FCM	96.09	0.93
	GIFP-FCM	96.88	0.94
	FKLICM	97.66	0.96
	MRFO-RBFNN	98.44	0.97

8 Conclusion

In this paper a semi supervised classifier for satellite images is designed. The proposed classifier is developed using an RBFNN which is a three-layer network. The network consists of an input layer, an output layer, and a hidden layer. The training phase is the most significant factor in the efficiency of any network. Therefore, in this paper the training of the network is done using the nature inspired algorithm known as the manta ray foraging optimization algorithm. The MRFO is inspired by the intelligent behaviour of manta rays. The classification

Table 8 Area coverage.

Class	Area covered (km^2)		
	Pre flooding	Post flooding	Change (post vs. pre)
Water	407.95	651.68	243.73 (+)
Vegetation	7699.14	7545.4	153.74 (−)
Built up area	539.17	449.23	89.94 (−)

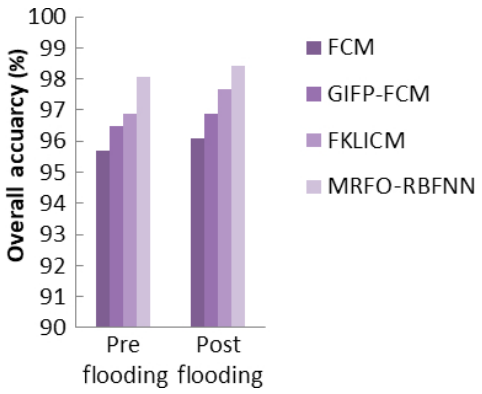

Fig. 9 Overall accuracy achieved by different methods.

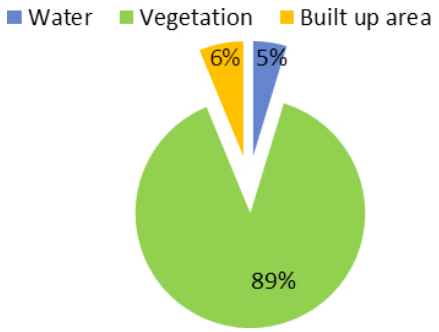

(a) Pre flooding

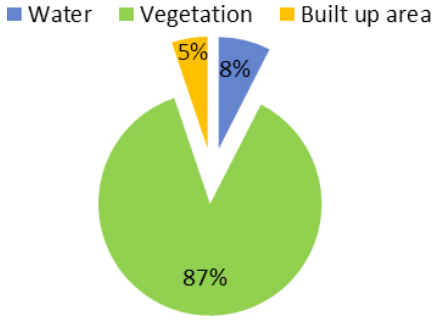

(b) Post flooding

Fig. 10 Percentage of land covers.

accuracy of the proposed method is high as the proposed training method improves the exploration. The proposed method is applied on pre and post satellite images of New Brunswick area. The classified images are used to detect the changes in the agriculture land and built-up area due to the flooding. The water cover of land increased whereas the agriculture land cover decreased. The accuracy assessment of the method is done using confusion matrix and producer and user accuracy. The kappa coefficient is also computed. The accuracy assessment reveals that the method works efficiently and can be used for identifying land cover classification and changes.

References

[1] K. K. Singh and A. Singh, Detection of 2011 Sikkim earthquake-induced landslides using neuro-fuzzy classifier and digital elevation model, *Natural Hazards*, vol. 83, no. 2, pp. 1027–1044, 2016.

[2] N. Kheradmandi and V. Mehranfar, A critical review and comparative study on image segmentation-based techniques for pavement crack detection, *Construction and Building Materials*, vol. 321, p. 126162, 2022.

[3] K. Liyanage and B. M. Whitaker, Feature analysis in satellite image classification using LC-KSVD and frozen dictionary learning, in *Proc. 2022 Intermountain Engineering, Technology and Computing* (*IETC*), Orem, UT, USA, 2022, pp. 1–6.

[4] K. K. Singh, M. J. Nigam, K. Pal, and A. Mehrotra, A fuzzy Kohonen local information C-means clustering for remote sensing imagery, *IETE Technical Review*, vol. 31, no. 1, pp. 75–81, 2014.

[5] S. Gxokwe, T. Dube, D. Mazvimavi, and M. Grenfell, Using cloud computing techniques to monitor long-term variations in ecohydrological dynamics of small seasonally-flooded wetlands in semi-arid South Africa, *Journal of Hydrology*, vol. 612, p. 128080, 2022.

[6] N. Mori, T. Takahashi, T. Yasuda, and H. Yanagisawa, Survey of 2011 Tohoku earthquake tsunami inundation and run-up, *Geophysical Research Letters*, vol. 38, no. 7, pp. 1–6, 2011.

[7] G. Amarnath, An algorithm for rapid flood inundation mapping from optical data using a reflectance differencing technique, *Journal of Flood Risk Management*, vol. 7, no. 3, pp. 239–250, 2013.

[8] S. M. Chignell, R. S. Anderson, P. Evangelista, M. J. Laituri, and D. M. Merritt, Multi-temporal independent component analysis and Landsat 8 for delineating maximum extent of the 2013 colorado front range flood, *Remote Sensing*, vol. 7, no. 8, pp. 9822–9843, 2015.

[9] W. K. Mun and L. Billa, Post-flood land use damage estimation using improved normalized difference flood index ($NDFI_3$) on Landsat 8 datasets: December 2014 floods, Kelantan, Malaysia, *Arabian Journal of Geosciences*, vol. 11, no. 15, p. 434, 2018.

[10] D. Lu and Q. Weng, A survey of image classification methods and techniques for improving classification performance, *International Journal of Remote Sensing*, vol. 28, no. 5, pp. 823–870, 2007.

[11] L. Zhu, F. -L. Chung, and S. Wang, Generalized fuzzy C-means clustering algorithm with improved fuzzy partitions, *IEEE Transactions on Systems, Man, and Cybernetics, Part B* (*Cybernetics*), vol. 39, no. 3, pp. 578–591, 2009.

[12] P. Wang, Pattern recognition with fuzzy objective function algorithms (James C. Bezdek), *SIAM Review*, vol. 25, no. 3, p. 442, 2013.

[13] K. K. Singh, M. J. Nigam, and K. Pal, Detection of 2011 Tohoku tsunami inundated areas in Ishinomaki city using generalized improved fuzzy Kohonen clustering network, *European Journal of Remote Sensing*, vol. 47, no. 1, pp. 461–475, 2014.

[14] A. Singh and K. K. Singh, Unsupervised change detection in remote sensing images using fusion of spectral and statistical indices, *The Egyptian Journal of Remote Sensing and Space Science*, vol. 21, no. 3, pp. 345–351, 2018.

[15] F. Schwenker, H. A. Kestler, and G. Palm, Three learning phases for radial-basis-function networks, *Neural Networks*, vol. 14, nos. 4&5, pp. 439–458, 2001.

[16] W. Zhao, Z. Zhang, and L. Wang, Manta ray foraging optimization: An effective bio-inspired optimizer for engineering applications, *Engineering Applications of Artificial Intelligence*, vol. 87, p. 103300, 2020.

[17] USGS, http://earthexplorer.usgs.gov, 2022.

[18] J. W. Jr. Rouse, R. H. Haas, J. A. Schell, and D. W. Deering, Monitoring vegetation systems in the Great Plains with ERTS, in *Third Earth Resources Technology Satellite-1 Symposium- Volume I: Technical Presentations, NASA SP-351*, S. C. Freden, E. P. Mercanti, and M. A. Becker, eds. Washington, DC, USA: NASA, 1974, pp. 309–317.

[19] A. R. Huete, A soil-adjusted vegetation index (SAVI), *Remote Sensing of Environment*, vol. 25, no. 3, pp. 295–309, 1988.

[20] H. Xu, Modification of normalised difference water index (NDWI) to enhance open water features in remotely sensed imagery, *International Journal of Remote Sensing*, vol. 27, no. 14, pp. 3025–3033, 2006.

[21] Y. Zha, J. Gao, and S. Ni, Use of normalized difference built-up index in automatically mapping urban areas from TM imagery, *International Journal of Remote Sensing*, vol. 24, no. 3, pp. 583–594, 2003.

[22] R. G. Congalton and K. Green, *Assessing the Accuracy of Remotely Sensed Data: Principles and Practices, Second Edition*. Boca Raton, FL, USA: CRC Press, 2008.

Amit Kumar Rai is an assistant professor in the Department of Electronics and Communication Engineering, Asansol Engineering College, India. He is currently pursing the PhD degree at the Department of Electronics Engineering, Indian Institute of Technology, Dhanbad (ISM, Dhanbad), India. He received the MTech degree from IIT (ISM), Dhanbad, India in 2009. His research and teaching areas are nano-electronics, artificial intelligence, communications, etc. He has published over 20 papers in peer reviewed journals and international conferences.

Krishna Kant Singh is working as a professor in the Department of CSE, ASET, Amity University, Noida, India. He has wide teaching and research experience. He has received the BTech, MTech, and PGD (ML&AI) degrees from IIIT Bangalore, and the PhD degree from IIT Roorkee in the area of image processing and remote sensing. He has authored more than 100 research papers in Scopus and SCIE indexed journals of repute. He has also authored 25 technical books. He is also an associate editor of *Journal of Intelligent & Fuzzy Systems* (SCIE indexed), *IEEE ACCESS* (SCIE indexed), and a guest editor of *Open Computer Science*, *Complex and Intelligent System* and *Microprocessors and Microsystems Journal*. He is also a member of editorial board of *Applied Computing & Geoscience* (Elsevier).

Nirupama Mandal received the BSc (Hons.) degree in physics, the BTech degree in instrumentation engineering, the MTech degree in instrumentation and control engineering, and the PhD (Tech.) degree in instrumentation engineering from University of Calcutta, Kolkata, India in 2001, 2004, 2006, and 2012, respectively. She has authored 37 papers in international journals and 20 papers in international conference proceedings. Her current research interests include transducer design, PC-based instrumentation, controller design, MEMS, and process modelling.

Ivan Izonin is working as an associate professor at the Department of Artificial Intelligence, Lviv Polytechnic National University, Lviv, Ukraine. He received the MSc degree in computer science from Lviv Polytechnic National University in 2011 and the MSc degree in economic cybernetics from Ivan Franko National University of Lviv in 2012. He received the PhD degree in artificial intelligence from Lviv Polytechnic National University in 2016. He has authored more than 125 publications, including 11 patents for inventions and 2 tutorials. His main research interests are focused on computational intelligence, high-speed neural-like systems, non-iterative machine learning algorithms, and image processing techniques.